JOURNAL OF THERMOPHYSICS AND HEAT TRANSFER
Vol. 10, No. 1, January–March 1996

Kinetics of the $N_2 + O \rightarrow NO + N$ Reaction Under Thermodynamic Nonequilibrium

Deepak Bose* and Graham V. Candler†
University of Minnesota, Minneapolis, Minnesota 55455

The first Zeldovich reaction, $N_2 + O \rightarrow NO + N$, plays a major role in nitric oxide formation in re-entry flows, combustion, and discharge flow systems. The kinetics of this reaction is uncertain under the strong thermodynamic nonequilibrium conditions and extremely high temperatures that often characterize these flows. We assess the influence of these conditions on the reaction rate using detailed quasiclassical trajectory calculations on the $^3A''$ surface obtained from ab initio contracted configuration interaction data. The effect of reactant energy modes on the rate constant is analyzed and a functional dependence of the rate constant on the vibrational, rotational, and translational temperatures is obtained. It is seen that strong nonequilibrium can reduce the rate constant by a factor of 5–6. In addition, the energy of the NO molecules formed by this reaction is determined and its dependence on the reagent energy is studied. The vibrational and rotational distributions of the product NO molecules under typical re-entry flow conditions are obtained and are found to be nearly Boltzmann. For strong nonequilibrium cases, NO is formed at high vibrational and rotational temperatures, in accordance with the bow-shock ultraviolet flight experiments.

Introduction

ACCURATE modeling of thermochemical phenomena in rarefied atmospheric flows remains a difficult problem.[1,2] Most current models fail at high altitudes because of the high degree of thermal nonequilibrium caused by infrequent molecular collisions. The limitations of the current models are illustrated by the first two bow-shock ultra-violet (BSUV) experiments, which flew at 3.5 and 5.1 km/s in the upper atmosphere.[3–6] These experiments measured the uv radiation emitted from the stagnation region shock layer. The theoretical estimates using state-of-the-art flow simulation codes were found to be 200 times lower than the experimental measurements. It was concluded that since the radiation spectrum was dominated by NO γ and β band emission, the large discrepancy was due to the predicted NO concentration being too low. A part of the difference was due to the breakdown of the continuum flow equations at high altitudes. On using the direct simulation Monte Carlo technique, Boyd et al.[7] found that the theoretical prediction was still 60 times lower than the measurements. In the BSUV flight regime, NO is primarily formed by the Zeldovich reactions[8]

$$\begin{aligned} N_2 + O &\rightarrow NO + N \\ O_2 + N &\rightarrow NO + O \end{aligned} \qquad (1)$$

and the first Zeldovich reaction is dominant. This reaction is driven by the availability of O atoms, which are obtained from the O_2 dissociation process. Boyd et al.[7] showed that using the Macheret and Rich vibration–dissociation coupling model[9,10] instead of the Park model[11,12] significantly improved the uv radiation predictions. However, they found that the theoretical predictions were still a factor of 2–4 in error. We expect that the remaining error is due to an improper treatment of the first Zeldovich reaction under strong nonequilibrium conditions.

Consider a typical BSUV2 stagnation region shock layer at an altitude of 80 km and a speed of 5.1 km/s. Figure 1 shows the computed translational, rotational, and vibrational temperature profiles along the stagnation streamline of this flow. Under these flight conditions, T_v and T_r are much lower than T_t due to finite rate internal energy relaxation. Under these strongly nonequilibrium conditions, the reaction rates are a function of the three temperatures. Many theories[9–14] have been proposed to predict the coupling between the dissociation and vibrational relaxation process. However, not many investigations have been carried out to estimate how thermal nonequilibrium affects the rates of the Zeldovich reactions.

Not only are the reaction rates affected by thermal nonequilibrium, but extensive analysis of the BSUV2 spectrally resolved radiation data has shown that the NO molecules have higher vibrational and rotational temperatures. Hence, it is essential to investigate how the energy is distributed among the energy modes when NO is formed by the Zeldovich reactions.

The first Zeldovich reaction will also be very important in the third flight of this series, BSUV3 or Skipper, which is to be flown at even higher altitudes (above 80 km). Under such conditions, there is a relatively high concentration of O atoms

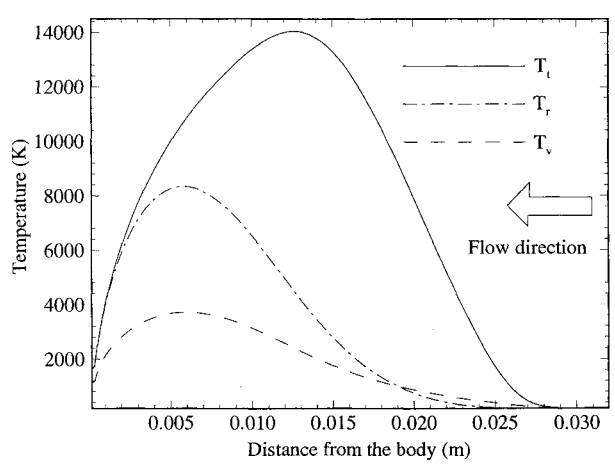

Fig. 1 Computed temperature profiles along the stagnation streamline of a 5.1-km/s flow at 80-km altitude.

Received July 3, 1995; revision received Oct. 3, 1995; accepted for publication Oct. 6, 1995.

*Graduate Student, Department of Aerospace Engineering and Mechanics. Member AIAA.

†Associate Professor, Department of Aerospace Engineering and Mechanics. Member AIAA.

in the freestream flow, and hence, the O_2 dissociation process is expected to play a smaller role in the NO formation mechanism. Therefore, the rate of NO formation is expected to be driven by the first Zeldovich reaction only and we need a better understanding of this reaction in highly nonequilibrium flows.

In this article we present a detailed study of the first Zeldovich reaction under thermal equilibrium and nonequilibrium conditions. Emphasis is given to investigating the effect of low T_v and T_r on the rate of the first Zeldovich reaction. In addition, we analyze the energy disposal among the products of this reaction. The results show that despite the NO being formed from an endothermic reaction, its vibrational and rotational temperatures are much higher than the average gas vibrational and rotational temperatures, in accordance with the experimental predictions. This can lead to a significant increase in electronically excited NO and radiative emission in the flowfield.

A quasiclassical trajectory[15-17] method (QCT) is chosen to study this reaction. This method is attractive because it yields the reaction rates at any initial state of the reactants and it provides useful insight into the details of the reaction process. A classical study is sufficiently accurate[15] for a high temperature gas of heavy nuclei. Also, the availability of an accurate ab initio potential energy surface[18,19] for this system makes this approach attractive. We use a quasiclassical technique in which the initial energies of the reactants are assumed quantized.

A quasiclassical trajectory study has been done for the second Zeldovich reaction[20] and the first reaction in the backward direction by Gilibert et al.[21,22] However, they have not presented any calculations under typical nonequilibrium flow conditions.

Potential Energy Surface

To obtain reliable results from the trajectory calculations, accurate potential energy surfaces are needed. Walch and Jaffe[18,19] present ab initio calculations of the potential energy surface (PES) joining the reactants and products in their ground electronic states for the Zeldovich reactions. For the first reaction, we have

$$N_2(X^1\Sigma_g^+) + O(^3P_g) \rightarrow N(^4S_u) + NO(X^2\Pi) \qquad (2)$$

In C_s symmetry the ground state reactants and products are adiabatically correlated through the two lowest lying triplet surfaces; $^3A''$ and $^3A'$.[23,24] The best estimate of the lowest energy barrier heights using the highest level of theory employed contracted configuration interaction (CCI) is 0.5 kcal/mol for $^3A''$ and 14.4 kcal/mol for $^3A'$ relative to the NO + N asymptote energy. The best estimate of the endothermicity from the ab initio calculations is 77 kcal/mol as compared to the experimental value of 75 kcal/mol. The $^3A''$ surface shows a bent saddle point configuration with a small energy barrier with respect to the NO + N asymptote at an NNO angle of 108.9 deg, strongly favoring noncollinear collisions. Imposing a collinear geometry increases the reaction energy barrier up to 0.81 eV with respect to the products. We assume that since the barrier height for the $^3A'$ surface lies well above that for the $^3A''$ surface, the reactivity for this endothermic reaction can be described using the $^3A''$ surface. The effect of the $^3A'$ surface is currently being included and will be presented in the future. An analytical representation of the $^3A''$ surface obtained by Gilibert et al.,[22] using a Sorbie–Murrell (SM) function[25,26] is used for the trajectory calculations.

Classical Trajectory Calculations

To study the dynamics of reaction (2) we solve the equations of motion for the NNO triatomic system. The appropriate form of the equations in the c.m. coordinate system is given elsewhere.[27] Six equations for positions and six for momenta are solved at every time step over the potential energy surface using a fourth-order Runge–Kutta[28] scheme with a constant time step. A trajectory code, written in CMFortran, is specifically developed for execution in data-parallel mode on the Thinking Machines CM-5. More than 100,000 trajectories are run in parallel for each case either on the 256- or 512-node partition of the CM-5. We obtain extremely high speedups compared to a purely scalar code since all trajectories are computed independently without any communications during the time integration. This allows us to compute a large batch of trajectories, which consequently, gives reaction attributes with small uncertainties.

Reaction Attributes

Reaction Cross Section

To calculate the reaction cross section one has to estimate a reasonable value of the maximum impact parameter $b_{\max}$, such that collisions with impact parameter $b > b_{\max}$ cannot possibly react. The reaction cross section is then defined as the product of the area $\pi b_{\max}^2$ and an average probability of reaction over all possible collisions. For atom–diatom collisions with relative translational energy E_t and diatom rovibrational state (v, j), the reaction cross section is given by[15-17]

$$\sigma_r(E_t, v, j) = \int_{\xi=0}^{2\pi}\int_{\eta=0}^{2\pi}\int_{\phi=0}^{2\pi}\int_{\theta=0}^{\pi}\int_{b=0}^{b_{\max}} \times P_r(b, \theta, \phi, \eta, \xi, E_t, v, j) 2\pi b \, db \frac{\sin\theta}{2} d\theta \frac{d\phi}{2\pi}\frac{d\eta}{2\pi}\frac{d\xi}{2\pi} \qquad (3)$$

where θ and ϕ define the orientation of the diatomic molecule, ξ represents the initial phase of vibration, and η describes the orientation of the angular momentum of the rotating diatom. The quantity P_r represents the probability of reaction under the given collision conditions. We use the Monte Carlo method to evaluate this multidimensional integral. In this method the previous integral is approximated by a summation

$$\sigma_r(E_t, v, j) = \frac{1}{N}\sum_N f(\bar{\beta}_i) \qquad (4)$$

where $f(\bar{\beta}_i)$ is a function of $\bar{\beta}_i$, the set of all collision parameters. This summation is evaluated using an appropriately large set of N trajectories. The probability function P_r is set equal to 1 if reaction occurs in a trajectory, otherwise it is set equal to 0. An importance-sampling[15,29] function is used to choose the impact parameter for each trajectory.

Thermal Rate Constant

A state-dependent thermal rate constant of reaction (2) can be obtained by averaging the reaction cross section over the Maxwellian translational energy distribution function at a given temperature.[15-17] Hence, we write

$$k_{v,j}(T) = \left(\frac{8k_BT}{\pi\mu_{N_2-O}}\right)^{1/2}\left(\frac{1}{k_BT}\right)^2\int_0^\infty \sigma_r(E_t, v, j)E_t \exp\left(\frac{-E_t}{k_BT}\right) dE_t \qquad (5)$$

where k_B is the Boltzmann constant and μ_{N_2-O} is the reduced mass for $N_2 - O$ collisions. The complete thermally averaged rate constant can now be obtained by averaging $k_{v,j}(T)$ over all internal energy states. For a gas in which the internal energy modes are in equilibrium with the translational energy modes, the rate constant can be written as a function of temperature T,

$$k(T) = \sum_v\sum_j g_j \frac{(2j+1)}{Q_{v-r}} \exp\left(\frac{-E_{v,j}}{k_BT}\right) k_{v,j}(T) \qquad (6)$$

Q_{v-r} is the vibrational–rotational partition function, and $E_{v,j}$ is the vibrational–rotational energy of N_2 in the v, j state. The factor g_j takes into account the nuclear spin degeneracy.

In the case where the vibrational and rotational modes are not equilibrated, we split the internal energy distribution in Eq. (6) into separate vibrational and rotational energy distribution functions under the anharmonic oscillator–rigid rotor approximation. This assumption of energy mode separability is good when the high vibrational levels are not dominant and is commonly employed in gasdynamics. Hence, the rate constant is given by

$$k(T) = \sum_v \frac{\exp(-E_v/k_BT)}{Q_v} \sum_j \frac{g_j(2j+1)\exp(-E_j/k_BT)}{Q_r} k_{v,j}(T) \tag{7}$$

The primary reason for decoupling the internal energy is to allow the vibrational and rotational levels to assume different distribution functions. However, once a set of v, j is chosen for a trajectory, the vibrational and rotational modes are treated in a fully coupled fashion during the time integration.

As discussed earlier, there exists a region of strong nonequilibrium behind a bow shock wave in a hypersonic flow. In this region the vibrational, rotational, and translational energies of the gas are characterized by different temperatures.[11] To calculate the rate constant under such conditions, we modify Eq. (7) to

$$k(T, T_v, T_r) = \sum_v \frac{\exp(-E_v/k_BT_v)}{Q_v} \times \sum_j \frac{g_j(2j+1)\exp(-E_j/k_BT_r)}{Q_r} k_{v,j}(T_t) \tag{8}$$

where Q_v and Q_r now are the respective partition functions at temperatures T_v and T_r, respectively. This will allow us to analyze the effect of T_v, T_r, and T_t on the thermal rate constant.

The product energy distribution[15] can be easily obtained by redefining P_r in Eq. (3) as $P_r(s)$, which is set equal to 1 only if N_2 and O react and form the product in state s. This gives us the product state-dependent rate constant, $k_s(T_t, T_v, T_r)$. The population of the product state s is now written as

$$N_s \propto k_s(T_t, T_v, T_r) \tag{9}$$

and we obtain a normalized product energy distribution.

Results and Discussion

Thermal Rate Constants

The temperature in a typical hypersonic flow may be as high as 30,000 K. To make reasonable predictions of the concentration of NO in the flowfield, experimental or theoretical rates are required at very high temperatures. Most of the experimental rates available are below T = 5000 K, a very few are between 5000–10,000 K, and none are above 10,000 K. In practice the computational fluid dynamics (CFD) flow simulations are made using empirical rate constants. These rates are obtained by extrapolating the experimental data using an Arrhenius expression. Since the extrapolation is done outside the range of experimental temperatures, the validity of these rates above 10,000 K is unknown.

The purpose of this section is to use the QCT method to predict the rate constant of reaction (2) over a wide temperature range. The calculations are done for this reaction with the reactants and products in the ground electronic state. Previously, only Jaffe et al.[30] have done a QCT study to predict the rate constant of the above reaction on the $^3A''$ PES. The agreement between the QCT and the experimental results seems very good in the narrow region of temperature where they

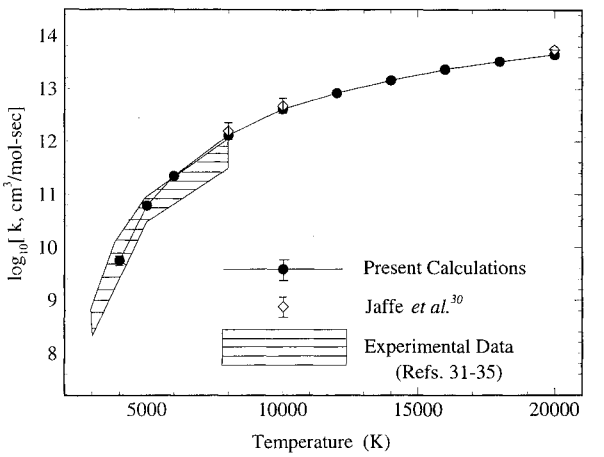

Fig. 2 Total thermal rate constant variation with temperature.

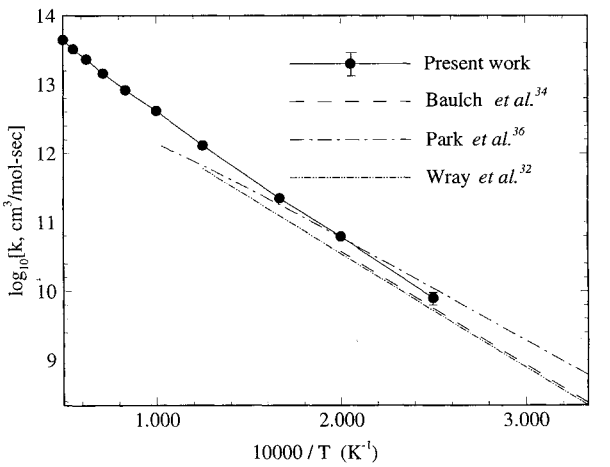

Fig. 3 Rate constant variation of the exchange reaction (2) with temperature.

overlap. However, they have not calculated many points between 5000–20,000 K to construct an analytical curve fit. In Fig. 2 we present the calculated total rate constant for the reaction over a temperature range of 4000–20,000 K. The calculations below a temperature of 4000 K show large statistical uncertainties, and hence, are not done. For each data point a large sample of more than 100,000 trajectories is run in data-parallel mode to restrict the statistical uncertainty below 4%, except at T = 4000 and 5000 K where the uncertainty is about 9%. The agreement between the experimental and the present calculations is very good between 4000–8000 K. The QCT results of Jaffe et al.[30] and the present calculations lie on the higher side of the experimental band. Ideally, one must also consider the presence of the electronic excited states of the reactants in the gas at T > 10,000 K, which could not be done here due to nonavailability of the appropriate ab initio PES.

Figure 3 compares the present QCT exchange rate constants with various experimental and empirical rate constants. Some of the early shock-tube predictions are given by Glick et al.[31] and Wray and Teare.[32] Duff and Davidson[33] successfully fit these kinetic data using the Arrhenius expressions, 5×10^{13} $\exp(-38{,}000/T)$ and 7.0×10^{13} $\exp(-38{,}000/T)$, respectively. Baulch et al.[34] recommend 7.6×10^{13} $\exp(-38{,}000/T)$ with an error factor of 2 in the range 2000–5000 K. Later, Monat et al.[35] obtain 1.84×10^{14} $\exp(-38{,}382/T)$ with an uncertainty of ±35% in the temperature range 2384–3850 K using a shock-tube technique. For atmospheric re-entry calculations Park et al.[36] recommend $6.4 \times 10^{17}T^{-1.0}$ $\exp(-38{,}370/T)$. The

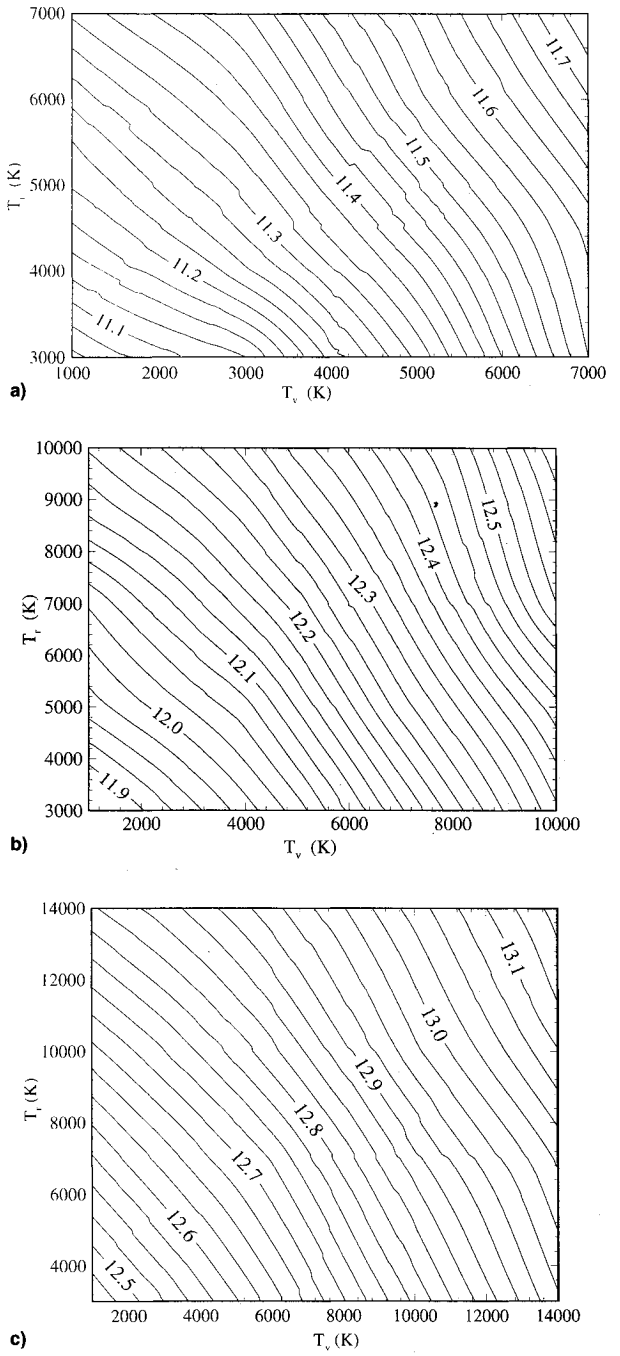

Fig. 4 Contour plots of $\log_{10}$ (k, cm^3/mol s) showing the effect of T_v and T_r on the rate constant of reaction (2). Twenty-five contours are drawn in each figure: a) T_t = 7000 K, contour spacing, $\Delta\log_{10}k$ = 0.025; b) T_t = 10,000 K, contour spacing, $\Delta\log_{10}k$ = 0.025; and c) T_t = 14,000 K, contour spacing, and $\Delta\log_{10}k$ = 0.025.

current QCT calculations yield the following expression for the exchange reaction rate constant:

$$k(T) = (4.5487 \pm 0.038) \times 10^{10} T^{0.8761 \pm 0.000934} \times \exp[(-35{,}991.4 \pm 77.55)/T] \quad \text{cm}^3/\text{mol s} \qquad (10)$$

between T = 4000–20,000 K. All of the recommended rate constants agree well with each other below T = 8000 K. For higher temperatures, the QCT rates and the empirical rates of Park et al.[36] diverge with the QCT curve giving larger rate constants. The larger rates at high temperatures give a positive power of the temperature in the pre-exponential factor of the rate constant expression. This partially explains the high NO concentration predicted by the BSUV2 experiment.[3–5]

Thermal Rate Constants for Nonequilibrium Flows

As discussed before, the flow in a shock layer formed in front of a blunt body is in nonequilibrium. This happens due to the sudden heating of the gas as it passes through the bow shock wave. The internal energy modes of the gas molecules, especially the vibrational mode, are not heated as quickly as the translational energy. As a result, the vibrational energy lags behind the rotational and the translational energy of the molecules. Under such conditions the different modes of energy are assumed to be distributed according to a nearly Boltzmann distribution, but with different characteristic temperatures.[11] When this assumption breaks down, an appropriate distribution function must be employed. From Fig. 1 it is clear that in hypersonic shock layers at high altitudes, $T_v < T_r \ll T_t$. To correctly model the thermochemical phenomenon in this region we must consider the fact that the rate constants of the reactions depend upon all three temperatures. However, the current empirical rate expressions for reaction (2) are a function of only one temperature T. Since the vibrational and rotational temperatures are typically less than T_t, these expressions may overpredict the reaction rates in the shock layer. It has been shown by several authors[1,10–14] that a low T_v has a very strong effect on the dissociation reaction rates. Hence, it is reasonable to expect that due to the low internal energy excitation of the molecules, the exchange reaction (2) will also be slowed down in a hypersonic flow. Moreover, this reaction is endothermic with a late potential barrier and is likely to be sensitive to internal energy changes.[37,38] Thus, it becomes important to analyze the effect of low T_v and T_r on the rate constant in the shock layer. In this section we compute the nonequilibrium reaction rate constants using Eq. (10). A set of a large number of trajectories (varying from 32,768 to 131,072) is run for each set of T_v, T_r, and T_t. The uncertainties in the rate constants are below 4%. Contour plots of the rate constants are made at T_t = 7000, 10,000, and 14,000 K (typical translational temperatures in the shock layer) in Fig. 4 vs T_v and T_r. T_v is varied from 1000 K to T_t, and T_r is varied from 3000 K to T_t. We plot 19 points in each figure to get the rate constant field, which is found to be sufficient since it is a very smooth function. At all three values of T_t considered, the difference between the maximum and the minimum point is around $10^{0.72}$. This shows that the rate constant is decreased by a factor of 5–6 due to large nonequilibrium ($T_v < T_r \ll T_t$). Although this is a significant factor, it is still less than what one expects, since the reaction (2) is believed to be more sensitive to the vibrational and rotational energy than the translational energy of the gas molecules. There are two primary reasons for this result. First, in this energy regime it is seen that all of the energy modes are equally efficient in increasing the reaction cross section. Second, to get the rate constants, the reaction cross sections are multiplied by a relative velocity factor, which is dependent on the translational temperature only. Also, the average relative translational energy of the reactants is more than the average vibrational or rotational energy, even when the gas is in equilibrium. Hence, T_t still governs the reaction rate of the first Zeldovich reaction, although T_v and T_r can reduce the reaction rate by a factor of 5–6 under nonequilibrium conditions.

To use these rate constants in CFD simulations, an analytical representation of the T_v, T_r dependence on the rates is required. In three dimensions, these surfaces look like a plane with a slight twist, which is adequately fit by the following expression:

$$\ell n\, k = aT_v + bT_r + cT_vT_r + d \qquad (11)$$

The coefficients a, b, c, and d are functions of translational temperature only. The rate constant expression as a function of T_v, T_r, and T_t may now be written as

$$k = \exp[-a(T_t - T_v) - b(T_t - T_r) - c(T_t^2 - T_rT_v)]AT_t^m \exp[-(D/T_t)] \quad \text{cm}^3/\text{mol-s} \qquad (12)$$

Table 1 Evaluated coefficients of Eq. (12) using a least-squares algorithm[a]

Coefficients	T_t = 7000 K	T_t = 10,000 K	T_t = 14,000 K
a	2.169×10^{-4}	1.449×10^{-4}	0.994×10^{-4}
b	1.789×10^{-4}	1.108×10^{-4}	0.747×10^{-4}
c	-8.951×10^{-9}	-3.279×10^{-9}	-2.475×10^{-9}
rms	0.012	0.014	0.0064

[a]The rms in the $\log_e$ scale is also given.

This expression is composed of two factors: 1) the Arrhenius rate expression for the equilibrium rate and 2) a factor dependent on T_t, T_v, and T_r for the nonequilibrium effect. The coefficients of the surface fit (12) are evaluated in Table 1 using a least-square fit in the $\log_e$ scale. A, m, and D are the regular Arrhenius parameters as evaluated in Eq. (10). Computations for more values of T_t are not presently done due to limited computational resources, however, they will be presented in the future. In Eq. (11) a T_vT_r term is added to take into account the twist in the surface. The twist arises due to the fact that the rate of increase of k with increasing T_r depends on the vibrational temperature of the gas, and vice versa. From Eq. (11) we can write

$$\frac{\partial\, \ell n\, k}{\partial T_r} = b + cT_v \tag{13}$$

Since $c < 0$, the effectiveness of T_r decreases with increasing T_v; the opposite also holds. Furthermore, since $a > b$, T_v is usually a little more effective than T_r.

When making thermochemical calculations for extremely rarefied flows, one should take into account the quick depletion of the population from the high-energy levels. This is especially important for the vibrational energy, since the vibrational energy equilibrates slowly. The molecules with high vibrational energy react faster than the rate of equilibration. As a result, there is a shortage of high-energy particles, leading to a non-Boltzmann distribution at high energy levels. This has an adverse effect on the reaction rates. To quantify the effect of the high vibrational energy molecules, we estimate the contribution of the upper half of the N_2 vibrational energy band ($E_v > 5$ eV) to the reaction rate constant. It is found that even in the most highly vibrationally excited gas considered at T_v = 14,000 K, the contribution of the high vibrational energy ($E_v > 5$ eV) N_2 molecules to the rate constant is no more than 11%. Also, in rarefied nonequilibrium flows, $T_v \ll T_t$, which restricts T_v below 4000 K in most low-density flow regimes. Under these conditions, the contribution of the high vibrationally excited molecules ($E_v > 5$ eV) to the reaction rate constant is less than 2%. Thus, the effect of the population depletion on the rate constant of reaction (2) can be safely ignored under the flow regimes considered. This also justifies the assumption of vibration–rotation mode separability, which is good for low vibrationally excited molecules.

Product Energy Disposal in Nonequilibrium Flows

In the previous section we presented some results showing how the rate of reaction (2) in a hypersonic flow is affected by nonequilibrium. The purpose of this section is to study the effect of nonequilibrium on the average state of the NO molecules formed due to this reaction. It is observed from the QCT study that different modes of energy of the gas are cooled or heated due to the reaction by different amounts depending on their initial availability. Here we estimate the average product energy in the vibrational and the rotational mode of the NO molecules formed due to reaction (2). We have already discussed that in nonequilibrium flows each mode of energy is characterized by a different temperature. Similar characterization is done to quantify the average energy of the product NO molecules. In other words, we estimate the vibrational and

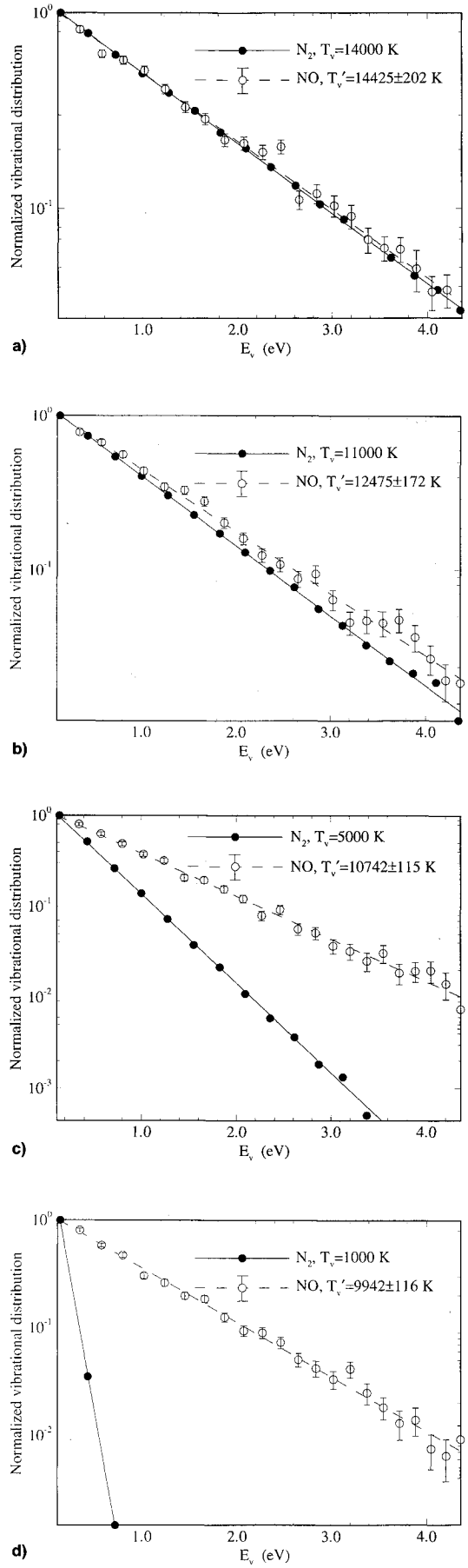

Fig. 5 Reactant and product vibrational distribution functions. T_t and T_r are fixed at 14,000 K. T_v = a) 14,000, b) 11,000, c) 5000, and d) 1000 K.

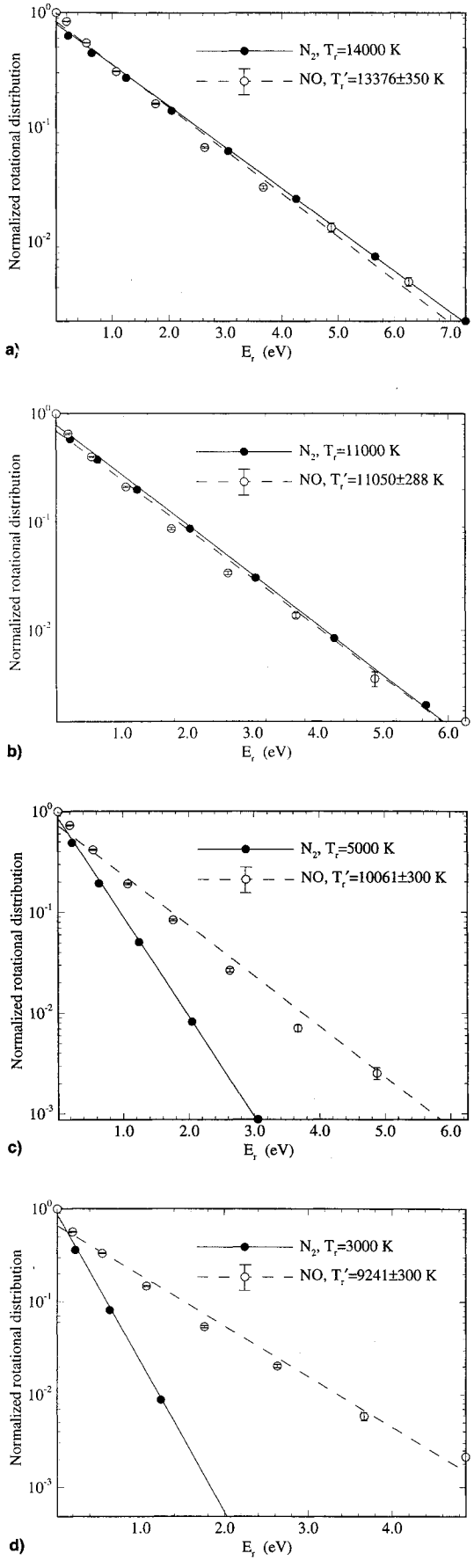

Fig. 6 Reactant and product rotational distribution functions. The reactant translational and vibrational temperatures are set at T_t = 14,000 K and T_v = 1000 K. T_r = a) 14,000, b) 11,000, c) 5000, and d) 3000 K.

the rotational temperatures of the NO molecules from their observed energy distributions. It is seen from the QCT analysis that the product NO molecules exhibit a Boltzmann-like distribution of the vibrational and the rotational energy. The vibrational energy distribution of the product molecules is written as

$$N_v = B_v \exp[-(E_v/kT'_v)] \tag{14}$$

In the previous expression B_v is a normalization factor and T'_v is the product vibrational temperature. Thus, we can compute T'_v from the product energy distribution. This function is plotted for different reactant vibrational temperatures T_v in Fig. 5.

The N_2 vibrational distribution function is also plotted for comparison. At high vibrational energy levels, where the values of N_v are small, a large scattering is observed. Hence, we plot E_v only up to 4.5 eV. However, this does not change the slope of the linear least-square fit, since the points scatter equally on both sides. It is clear from Fig. 5 that the product vibrational temperature T'_v is higher than the reactant vibrational temperature. This phenomenon is prominent under nonequilibrium flow conditions where $T_v \ll T_t$. This clearly shows that at low reactant vibrational temperatures, a heating of the vibrational energy mode of the gas is observed. Figure 5a shows that a little heating of the vibrational mode occurs even in the equilibrium flow conditions ($T_t = T_v = T_r$). Consequently, most of the endothermicity of the reaction is derived from the translational mode, leading to a translational cooling of the gas. Hence, in a CFD flow simulation, the NO produced from the first Zeldovich mechanism should be assigned a different vibrational temperature, as it is produced vibrationally very hot in the flow where $T_v \ll T_t$. These vibrationally hot NO molecules can be easily excited to the higher electronic states.

A similar trend is seen for the rotational energy distribution of the product NO molecules. The rotational energy also follows a near-Boltzmann distribution. Hence, we can write

$$N_j = B_r(2j + 1)\exp[-(E_r/kT'_r)] \tag{15}$$

where B_r is a normalization factor and T'_r is product rotational temperature. T'_r is obtained from the slope of the $\ell n(N_j/2j + 1)$ vs E_r curve. This function is plotted in Fig. 6. Since the rotational levels are closely spaced, we bin 10 levels together to reduce the statistical uncertainty. The plots show a nearly linear behavior at all rotational temperatures chosen. T_t and T_v are fixed at 14,000 and 1000 K, respectively. We observe that as the reactant rotational temperature decreases, a heating of the rotational mode is observed. At high rotational nonequilibrium T'_r is much higher than T_r. This analysis, therefore, shows that under nonequilibrium conditions the NO produced from the first Zeldovich reaction is rotationally hot.

The previous results show that, since the NO molecules formed from reaction (2) are vibrationally and rotationally very hot, they can be readily excited by collisions (or a photon) to NO(A) or NO(B). This could explain the BSUV experimental predictions of a large uv emission from the NO γ and β systems.

Conclusions

A detailed quasiclassical trajectory study for the first Zeldovich reaction is done. The rate constants obtained from the study agree well with the current experimental and empirical data. The QCT results of Jaffe et al.[30] also match the current results. An Arrhenius rate expression, based on this study, is also obtained for the first Zeldovich reaction with a positive temperature exponent in the pre-exponential factor. This partially explains the high NO concentration in the BSUV flowfield. We also note that strong nonequilibrium ($T_v < T_r \ll T_t$)

for the nonequilibrium rate constant as a function of T_r, T_v, and T_t is also obtained. We also find that the NO formed from the first Zeldovich reaction is vibrationally and rotationally very hot. These internally hot NO(X) molecules can easily be excited to NO(A) and NO(B) states, further explaining the experimental predictions of high uv emission from the NO γ and β systems.

Acknowledgments

Support for the authors is provided by the Army Research Office under Grant DAAH04-93-G-0089. This work was also sponsored in part by the Army High Performance Computing Research Center under the auspices of the Department of the Army, Army Research Laboratory cooperative agreement DAAH04-95-2-0003/contract DAAH04-95-C-0008, the content of which does not necessarily reflect the position or the policy of the government, and no official endorsement should be inferred.

References

[1]Park, C., *Thermal Design of Aeroassisted Orbital Transfer Vehicles*, edited by H. F. Nelson, Vol. 96, Progress in Astronautics and Aeronautics, AIAA, New York, 1985, pp. 511–537.

[2]Jaffe, R. L., *Thermophysical Aspects of Re-Entry Flows*, edited by J. N. Moss and C. D. Scott, Vol. 96, Progress in Astronautics and Aeronautics, AIAA, New York, 1986, pp. 123–151.

[3]Levin, D. A., Candler, G. V., Collins, R. J., Erdman, P. W., Zipf, E. C., and Howlett, C., "Examination of Theory for Bow Shock Ultraviolet Rocket Experiments—I," *Journal of Thermophysics and Heat Transfer*, Vol. 8, No. 3, 1994, pp. 447–452.

[4]Levin, D. A., Braunstein, M., Candler, G. V., Collins, R. J., and Smith, G., "Examination of Theory for Bow Shock Ultraviolet Rocket Experiments—II," *Journal of Thermophysics and Heat Transfer*, Vol. 8, No. 3, 1994, pp. 453–459.

[5]Levin, D. A., Candler, G. V., Collins, R. J., Erdman, P. W., Zipf, E. C., Espy, P., and Howlett, C., "Comparison of Theory with Experiment for the Bow Shock Ultraviolet Rocket Flight," *Journal of Thermophysics and Heat Transfer*, Vol. 7, No. 1, 1993, pp. 30–36.

[6]Erdman, P. W., Zipf, E. C., Espy, P., Howlett, C., Levin, D. A., Collins, R. J., and Candler, G. V., "Measurements of Ultraviolet Radiation from a 5 km/s Bow Shock," *Journal of Thermophysics and Heat Transfer*, Vol. 8, No. 3, 1994, pp. 441–446.

[7]Boyd, I. D., Candler, G. V., and Levin, D. A., "Dissociation Modeling in Low Density Hypersonic Flows of Air," *Physics of Fluids*, Vol. 7, No. 7, 1995, pp. 1757–1763.

[8]Zeldovich, Ya. B., Sadovnikov, P. Ya., and Frank-Kamenetskii, D. A., *Oxidation of Nitrogen in Combustion*, Academy of Sciences of USSR, Inst. of Chemical Physics, Moscow–Leningrad (translated by M. Shelef), 1947.

[9]Macheret, S. O., and Rich, J. W., "Nonequilibrium Dissociation Rates Behind Strong Shock Waves: Classical Model," *Chemical Physics*, Vol. 174, 1993, pp. 25–43.

[10]Macheret, S. O., Fridman, A. A., Adamovich, I. V., Rich, J. W., and Treanor, C. E., "Mechanisms of Nonequilibrium Dissociation of Diatomic Molecules," AIAA Paper 94-1984, June 1994.

[11]Park, C., *Nonequilibrium Hypersonic Aerothermodynamics*, Wiley, New York, 1990.

[12]Park, C., "Assessment of Two-Temperature Kinetic Model for Dissociating and Weakly Ionizing Nitrogen," *Journal of Thermophysics and Heat Transfer*, Vol. 2, No. 1, 1988, pp. 8–16.

[13]Hammerling, P., Teare, J. D., and Kivel, B., "Theory of Radiation from Luminous Shock Waves in Nitrogen," *Physics of Fluids*, Vol. 2, No. 4, 1959, pp. 422–426.

[14]Treanor, C. E., and Marrone, P. V., "Effect of Dissociation on the Rate of Vibrational Relaxation," *Physics of Fluids*, Vol. 5, No. 9, 1962, pp. 1022–1026.

[15]Truhlar, D. G., and Muckerman, J. T., "Reactive Scattering Cross Sections III: Quasiclassical and Semiclassical Methods," *Atom Molecule Collision Theory*, edited by R. B. Bernstein, Plenum, New York, 1979, pp. 505–561.

[16]Porter, R. N., and Raff, L. M., "Classical Trajectory Methods in Molecular Collisions," *Dynamics of Molecular Collisions Part B*, edited by W. H. Miller, Plenum, New York, 1976, pp. 1–50.

[17]Karplus, M., Porter, R. N., and Sharma, R. D., "Exchange Reactions with Activation Energy," *Journal of Chemical Physics*, Vol. 43, No. 9, 1965, pp. 3259–3287.

[18]Walch, S. P., and Jaffe, R. L., "Calculated Potential Surfaces for the Reactions: $O + N_2 \rightarrow NO + N$ and $N + O_2 \rightarrow NO + O$," *Journal of Chemical Physics*, Vol. 86, No. 12, 1987, pp. 6946–6956.

[19]Walch, S. P., and Jaffe, R. L., American Inst. of Physics Document PAPS JCPSA-86-6946-10.

[20]Gilibert, M., Aguilar, A., González, M., and Sayós, R., "Quasiclassical Trajectory Study of the $N(^4S_u) + O_2(X^3\Sigma_g^-) \rightarrow NO(X^2\Pi) + O(^3P_g)$ Atmospheric Reaction on the $^2A'$ Ground Potential Energy Surface Employing an Analytical Sorbie-Murrell Potential," *Chemical Physics*, Vol. 172, 1993, pp. 99–115.

[21]Gilibert, M., Aguilar, A., González, M., and Sayós, R., "Dynamics of the $N(^4S_u) + NO(X^2\Pi) \rightarrow N_2(X^1\Sigma_g^+) + O(^3P_g)$ atmospheric reaction on the $^3A''$ ground potential energy surface. II. Analytical potential energy surface and preliminary quasiclassical trajectory calculations," *Journal of Chemical Physics*, Vol. 99, No. 3, 1993, pp. 1719–1733.

[22]Gilibert, M., Aguilar, A., González, M., Mota, F., and Sayós, R., "Dynamics of the $N(^4S_u) + NO(X^2\Pi) \rightarrow N_2(X^1\Sigma_g^+) + O(^3P_g)$ Atmospheric Reaction on the $^3A''$ Ground Potential Energy Surface. I. Analytical Potential Energy Surface and Preliminary Quasiclassical Trajectory Calculations," *Journal of Chemical Physics*, Vol. 97, No. 8, 1992, pp. 5542–5553.

[23]Donovan, R. J., and Hussain, D., "Recent Advances in the Chemistry of Electronically Excited Atoms," *Chemical Reviews*, Vol. 70, No. 4, 1970, pp. 489–516.

[24]Hopper, D. G., "*Ab initio* Multiple Root Optimization MCSCF Study of the $C_{\infty v}/C_s$ Excitation Spectra and Potential Energy Surfaces of N_2O," *Journal of Chemical Physics*, Vol. 80, No. 9, 1984, pp. 4290–4316.

[25]Sorbie, K. S., and Murrell, J. N., "Analytical Potentials for Triatomic Molecules from Spectroscopic Data," *Molecular Physics*, Vol. 29, No. 5, 1975, pp. 1387–1407.

[26]Murrell, J. N., Carter, S., Farantos, S. C., Huxley, P., and Varandas, A. C. J., *Molecular Potential Energy Functions*, Wiley, London, 1984.

[27]Hirst, D. M., *Potential Energy Surfaces: Molecular Structure and Reaction Dynamics*, Taylor and Francis, London, 1985.

[28]Burden, R. L., and Faires, J. D., *Numerical Analysis*, PWS–Kent Publishing Co., Boston, MA, 1989.

[29]Faist, M. B., Muckerman, J. T., and Schubert, F. E., "Importance Sampling and Histogrammic Representations of Reactivity Functions and Product Distributions in Monte Carlo Quasiclassical Trajectory Calculations," *Journal of Chemical Physics*, Vol. 69, No. 9, 1978, pp. 4087–4096.

[30]Jaffe, R. L., Pattengill, M. D., and Schwenke, D. W., "Classical Trajectory Studies of Gas Phase Reaction Dynamics and Kinetics Using *Ab Initio* Potential Energy Surfaces," *Supercomputer Algorithms for Reactivity, Dynamics and Kinetics of Small Molecules*, edited by A. Lagná, Kluwer, Dordrecht, The Netherlands, 1989.

[31]Glick, H. S., Klein, J. J., and Squire, W., "Single-Pulse Shock Tube Studies of the Kinetics of the Reaction $N_2 + O_2 \rightleftharpoons 2NO$ Between 2000–3000°K," *Journal of Chemical Physics*, Vol. 27, No. 4, 1957, pp. 850–857.

[32]Wray, K. L., and Teare, J. D., "Shock-Tube Study of the Kinetics of Nitric Oxide at High Temperatures," *Journal of Chemical Physics*, Vol. 36, No. 10, 1962, pp. 2582–2596.

[33]Duff, R. E., and Davidson, N., "Calculation of Reaction Profiles Behind Steady State Shock Waves II. The Dissociation of Air," *Journal of Chemical Physics*, Vol. 31, No. 4, 1959, p. 1018.

[34]Baulch, D. L., Drysdale, D. D., and Haine, D. G., *Evaluated Kinetic Data for High Temperature Reactions*, Vol. 2, Butterworths, London, 1973.

[35]Monat, J. P., Hanson, R. K., and Kruger, C. H., "Shock Tube Determination of the Rate Coefficient for the Reaction $N_2 + O \rightarrow NO + N$," *Proceedings of the 17th Symposium (International) on Combustion*, The Combustion Inst., Pittsburgh, PA, 1978, p. 543.

[36]Park, C., Howe, J. T., Jaffe, R. L., and Candler, G. V., "Review of Chemical-Kinetic Problems of Future NASA Missions, II: Mars Entries," *Journal of Thermophysics and Heat Transfer*, Vol. 8, No. 1, 1994, pp. 9–23.

[37]Levine, R. D., and Bernstein, R. B., *Molecular Reaction Dynamics and Chemical Reactivity*, Oxford Univ. Press, New York, 1987.

[38]Duff, J. W., and Truhlar, D. G., "Effect of Curvature of the Reaction Path on Dynamic Effects in Endothermic Chemical Reactions and Product Energies in Exothermic Reactions," *Journal of Chemical Physics*, Vol. 62, No. 6, 1975, pp. 2477–2491.